Supporting Information for

Steady-state crystal nucleation rate of polyamide 66 by combining atomic force microscopy and fast scanning chip calorimetry

Rui Zhang[1], Evgeny Zhuravlev[1,2,3], Jürn W.P. Schmelzer[1], René Androsch[4], Christoph Schick[1,5,*]

[1] Institute of Physics and Competence Centre °CALOR, University of Rostock, 18051 Rostock, Germany

[2] Department of Polymer Science and Engineering, School of Chemistry and Chemical Engineering, Key Laboratory of High-Performance Polymer Materials and Technology of Ministry of Education, and The State Key Laboratory of Coordination Chemistry, Nanjing University, Nanjing 210093, China

[3] Shenyang Research Institute, Nanjing University, Shenyang 224300, China

[4] Interdisciplinary Center for Transfer-oriented Research in Natural Sciences (IWE TFN), Martin Luther University Halle-Wittenberg, 06099 Halle/Saale, Germany

[5] Butlerov Institute of Chemistry, Kazan Federal University, 18 Kremlyovskaya Street, Kazan 420008, Russia

[*] christoph.schick@uni-rostock.de

Section 1: Reproducibility of AFM images

Figure S1 shows some of the additional AFM phase images, which have been used to check reproducibility of the determined number of crystals and to obtain the error bar for the data points in Figure 8 of the main text. The experiments follow the method illustrated in Figure 3A of the main text.

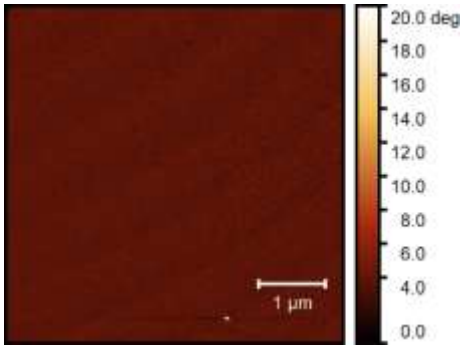

(A) 2 s

Num_{cryst}: 2, $N_v(t)$: 8.00×10^{17} m^{-3}

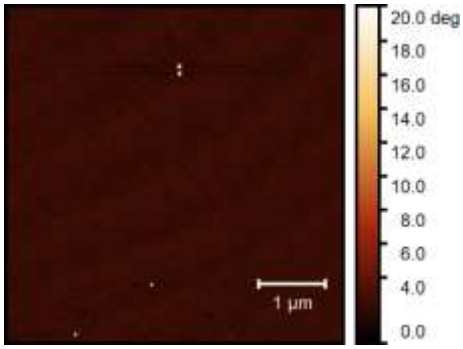

(B) 4 s

Num_{cryst}: 4, $N_v(t)$: 1.60×10^{18} m^{-3}

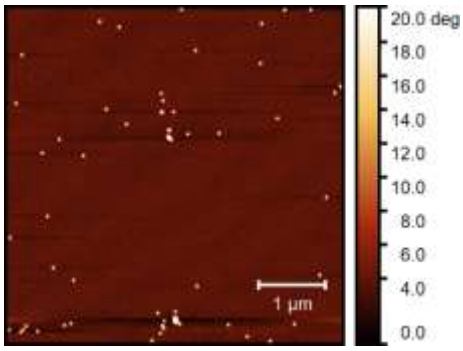

(C) 10 s

Num_{cryst}: 55, $N_v(t)$: 2.20×10^{19} m^{-3}

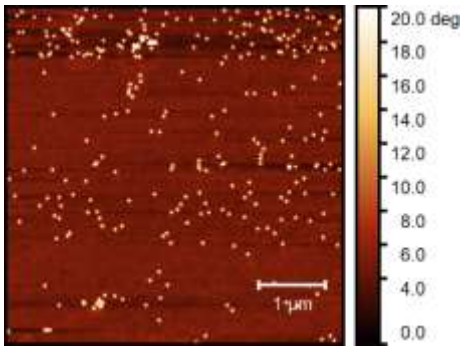

(D) 20 s

Num_{cryst}: 207, $N_v(t)$: 8.28×10^{19} m^{-3}

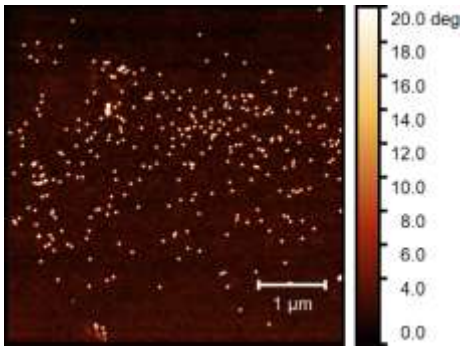

(E) 40 s

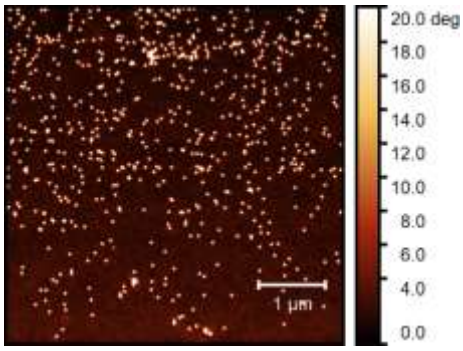

(F) 100 s

Num_{cryst}: 295, $N_v(t)$: 1.18×10^{20} m^{-3}

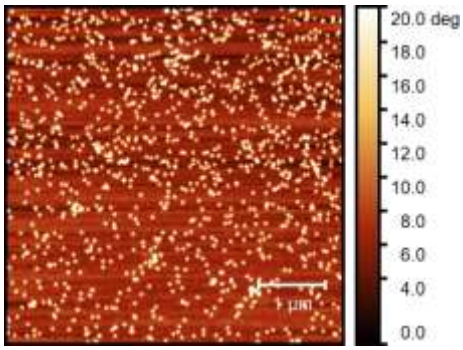

(G) 200 s

Num_{cryst}: 750, $N_v(t)$: 3.00×10^{20} m^{-3}

Num_{cryst}: 548, $N_v(t)$: 2.19×10^{20} m^{-3}

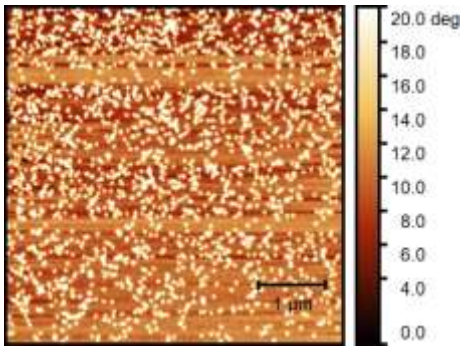

(H) 400 s

Num_{cryst}: 1116, $N_v(t)$: 4.46×10^{20} m^{-3}

Figure S1 AFM phase images of PA 66 after thermal treatments as shown in Figure 3A of the main text. Annealing temperature times. (A) 2 s, (B) 4 s, (C) 10 s, (D) 20 s, (E) 40 s, (F) 100 s, (G) 200 s, (H) 400 s.

Section 2: Number density of nuclei from AFM images through ImageJ software

This section shows how to process the data for estimating the number of crystals in the AFM images and estimating the number density of nuclei. The AFM images are stored in the RGB-color scheme. The RGB color scheme is an additive color model in which red, green, and blue are combined in various ways to reproduce a broad array of colors. Unfortunately, the software cannot distinguish the crystalline and amorphous phases through the brightness of the spots in the images. By transferring the RGB-color images to a 8-bit color scheme with black and white contrast this becomes possible. The crystals and amorphous phases are finally represented by white and black color, respectively. Figure S2 shows an example of transferring a RGB-color image (A) to a 8-bit color image (B).

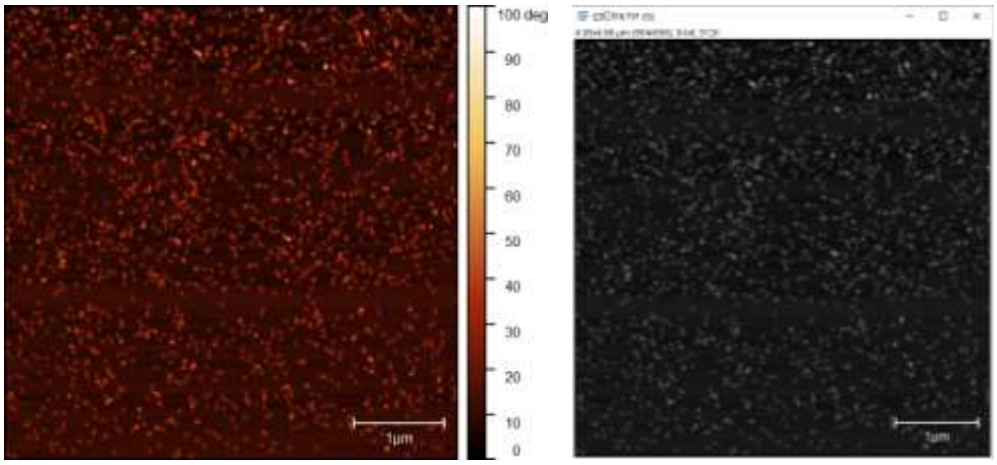

(A) (B)

Figure S2 Example of pre-processing AFM images to adapt them to ImageJ software. The image of Figure 7L from the main text is applied to illustrate the procedure. (A) AFM image (RGB color scheme); (B) AFM image after transformation to the 8-bit color scheme.

In the 8-bit color image, the crystals can be identified and captured by the ImageJ software. Contrast is further enhanced by changing grey to red as in Figure S3A. The corresponding result for the crystal number, 1263, is shown in Figure S3B.

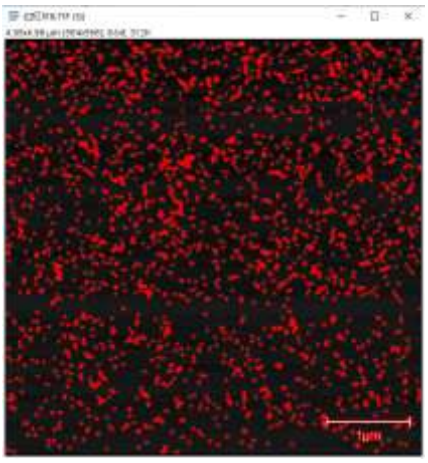

(A)

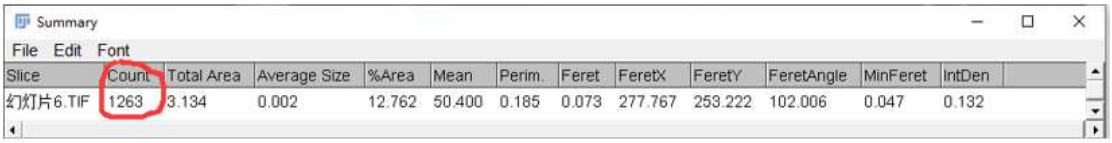

Summary

File Edit Font

Slice	Count	Total Area	Average Size	%Area	Mean	Perim.	Feret	FeretX	FeretY	FeretAngle	MinFeret	IntDen
幻灯片6.TIF	1263	3.134	0.002	12.762	50.400	0.185	0.073	277.767	253.222	102.006	0.047	0.132

(B)

Figure S3 (A) Example of identifying the crystals in the AFM images by ImageJ software. Crystals are marked in red color. (B) Results of ImageJ analysis. The red circle highlights the obtained crystal number in the 25 μm^2 image area.

Figure S4 (A)-(F) shows the identification of crystals in the AFM images corresponding to Figure 7 (G)-(L) of the main text through the ImageJ software.

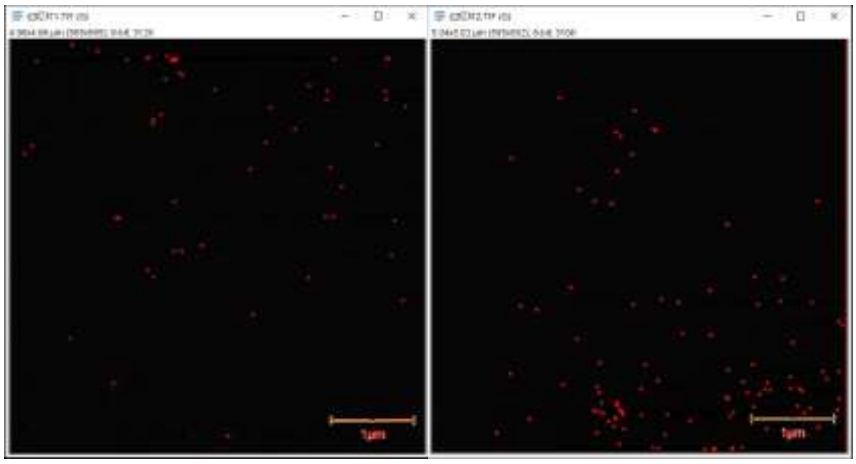

(A) (B)

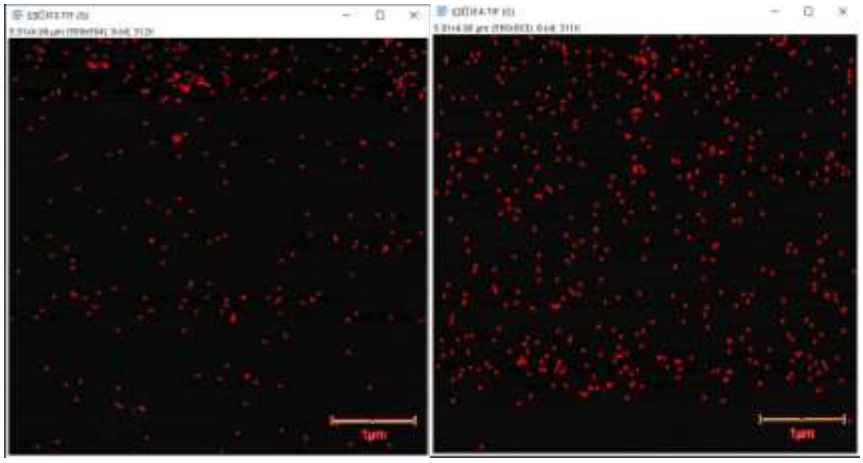

(C) (D)

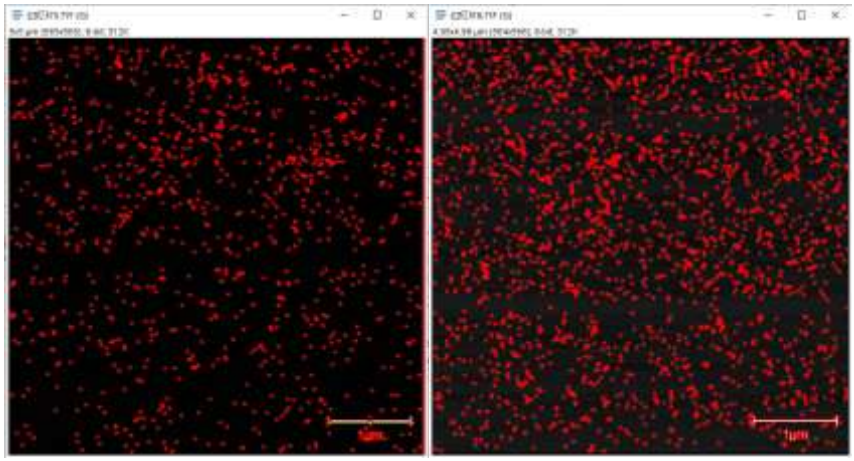

(E) (F)

Figure S4 Identifying the crystals in AFM images by ImageJ software. (A)-(F) corresponds to Figure 7 (G)-(L) of the main text, respectively.

The number of crystals in average and their corresponding nuclei densities are listed in Table S1. The nuclei densities ($N_v(t)$) are estimated through

$$N_v(t) = \frac{n(t)}{A_{area} \times L_{thickness}} \quad \text{(S1)}$$

where $n(t)$ is the number of crystals observed in the AFM images after annealing for a particular time t, A_{area} is the area of the AFM image (25 μm^2). As shown in Figure S4, the diameter of the crystals is about 0.1 μm. We assume in each layer with the thickness of 0.1 μm the crystal number is equal to the number of crystals observed by AFM. Therefore, $L_{thickness}$, the thickness containing the observed crystals, is assumed 0.1 μm. With this assumption, the nuclei density in the three-dimensional space can be estimated through Eq.(S1).[1]

Table S1. The number of crystals in AFM images after annealing at 310 K and estimated nuclei density through Eq.(S1).

Annealing time in s	Average number of crystals	Nuclei density in m^{-3}
1	2*	8.0×10^{17}
2	3*	1.2×10^{18}
4	5*	2.0×10^{18}
10	55	2.2×10^{19}
20	94	3.8×10^{19}
40	259	1×10^{20}
100	421	1.7×10^{20}
200	795	3.2×10^{21}
400	1220	4.9×10^{21}

*counted by eyes.

Section 3: Influence of the FSC oven (starting) temperature on the observed enthalpy changes

In the combined AFM-FSC setup, the oven temperature is limited to 278 K by the AFM. In a dedicated FSC setup, the oven temperature was set to 83 K. In both cases, the oven temperature determines the starting temperature of the heating scans. The influence of these different starting temperatures on the quality of the heating curves was studied.

Isothermal crystallization experiments were performed and the corresponding FSC heating curves are shown in Figure S5 (A) and (B) for the oven temperatures of 278 K and 83 K, respectively. The corresponding results for the cold-crystallization enthalpy are shown in Figure S5 (C) and (D). The data obtained from FSC with an oven temperature of 83 K display a better linearity than the data at 278 K because of better stability of the curves starting at 83 K. This influences the linearity of the enthalpy data at short annealing times. Nevertheless, the linear fits yield similar slopes for the time dependencies within the first 20 s.

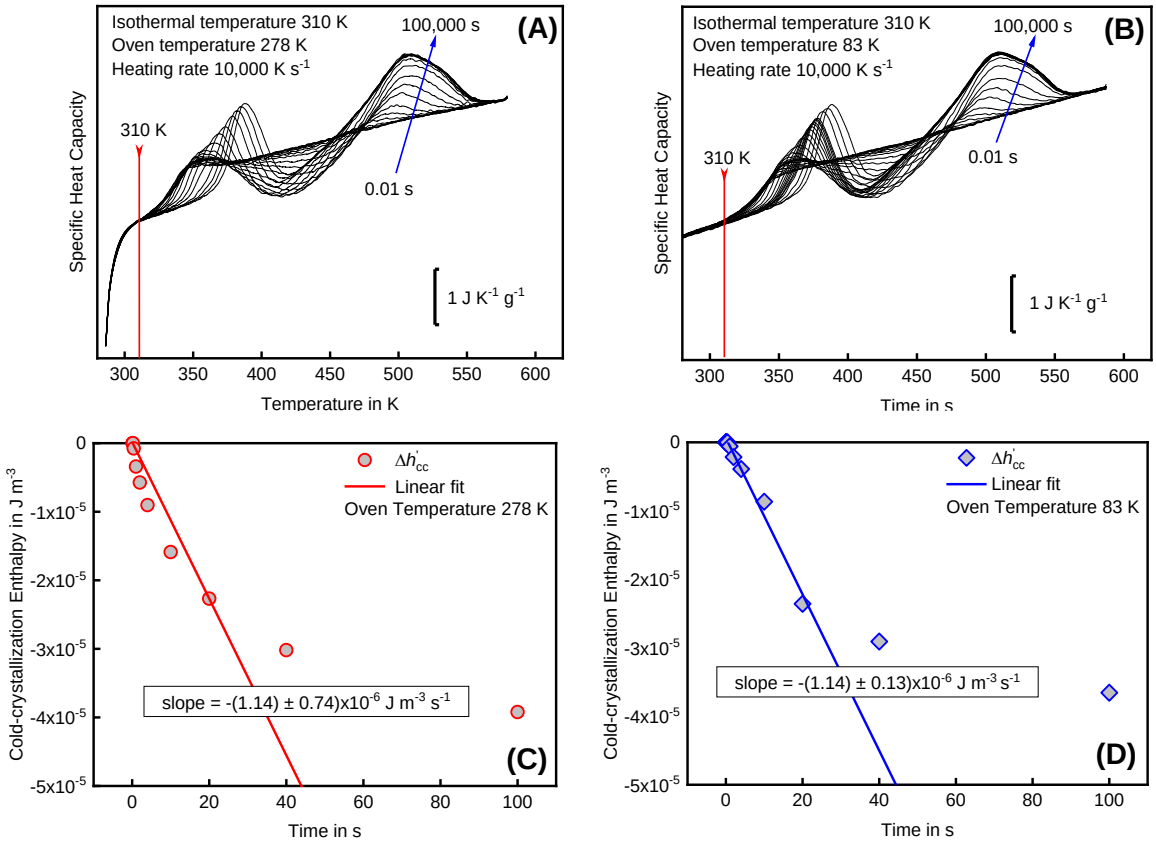

Figure S5 Specific heat capacity against temperature with oven temperatures 278 K (A) and 83 K (B). Enthalpy change of cold-crystallization against annealing time with oven temperatures 278 K (C) and 83 K (D).

Section 4: FSC curves after annealing at different temperatures

Figure S6 shows the FSC reheating curves after annealing at different temperatures from 315 to 420 K, which corresponds to the green segment in Figure 9 of the main text. The annealing time for annealing temperatures from 310 to 325 K are between 0.01 and 100,000 s, and the annealing time for annealing temperatures from 330 to 420 K are between 0.01 and 10,000 s.

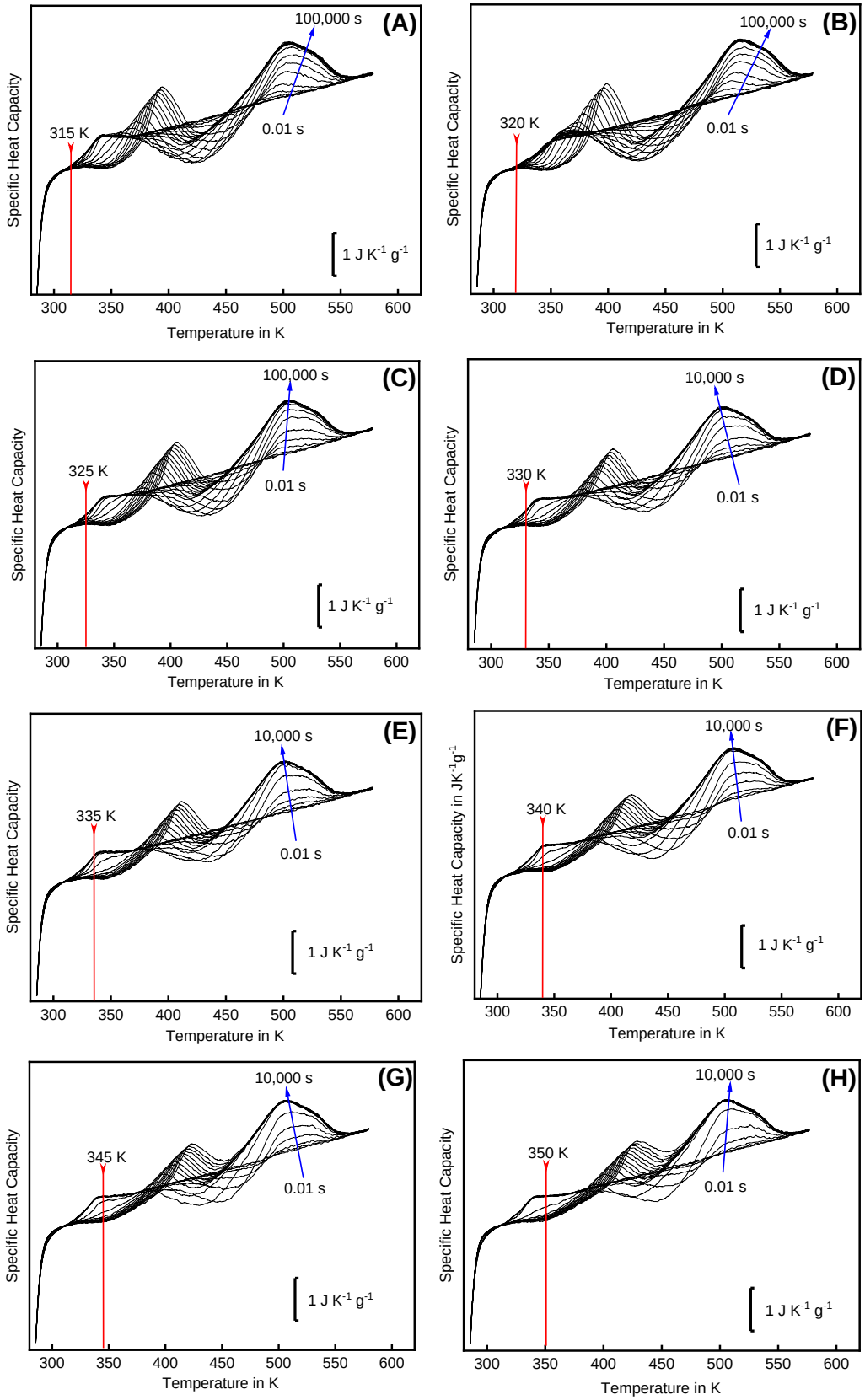
(A)
100,000 s
0.01 s
315 K
1 J K-1 g-1
Specific Heat Capacity
Temperature in K
(B)
100,000 s
0.01 s
320 K
1 J K-1 g-1
Specific Heat Capacity
Temperature in K
(C)
100,000 s
0.01 s
325 K
1 J K-1 g-1
Specific Heat Capacity
Temperature in K
(D)
10,000 s
0.01 s
330 K
1 J K-1 g-1
Specific Heat Capacity
Temperature in K
(E)
10,000 s
0.01 s
335 K
1 J K-1 g-1
Specific Heat Capacity
Temperature in K
(F)
10,000 s
0.01 s
340 K
1 J K-1 g-1
Specific Heat Capacity in JK-1g-1
Temperature in K
(G)
10,000 s
0.01 s
345 K
1 J K-1 g-1
Specific Heat Capacity
Temperature in K
(H)
10,000 s
0.01 s
350 K
1 J K-1 g-1
Specific Heat Capacity
Temperature in K
300
350
400
450
500
550
600

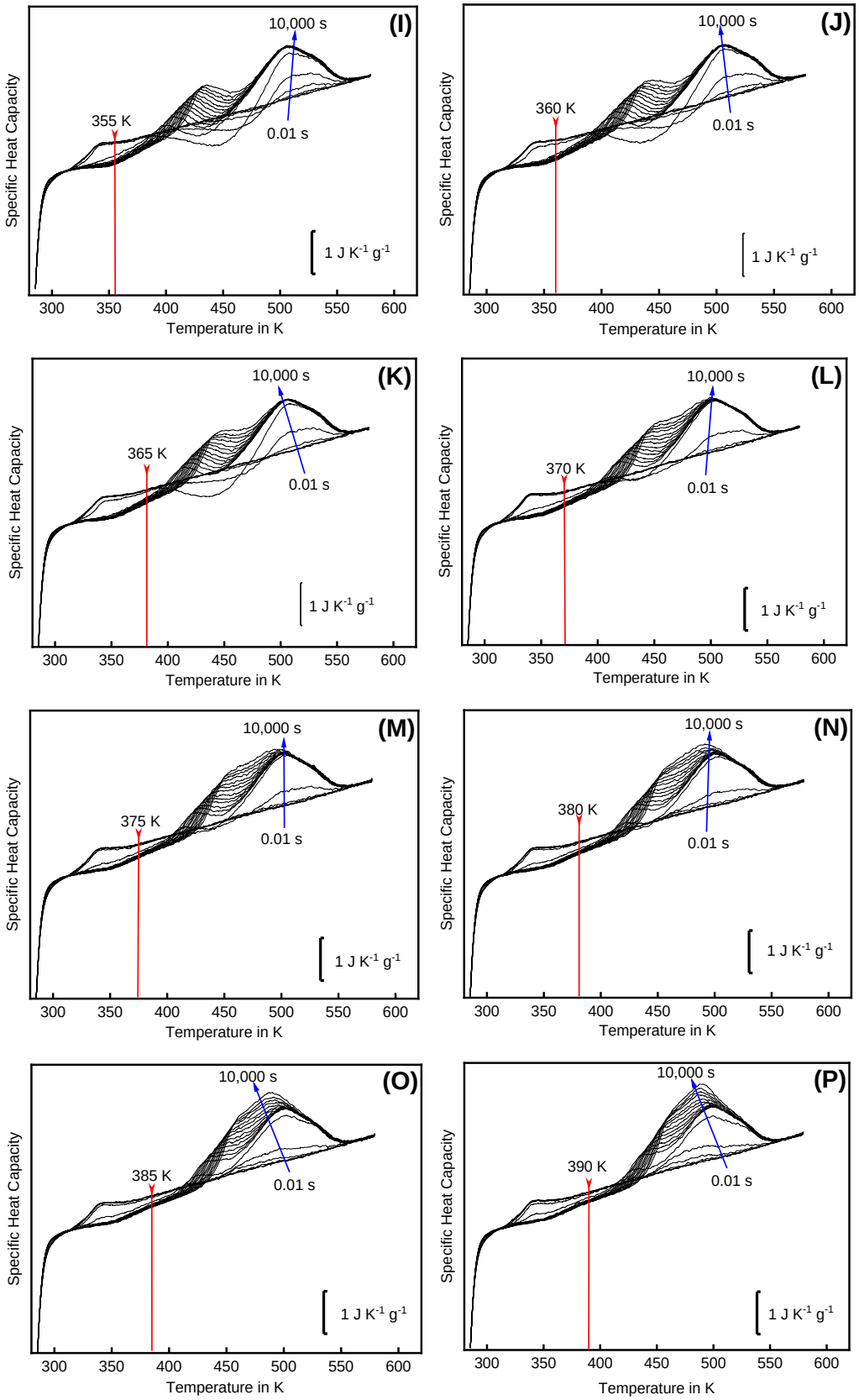
(I)
10,000 s
0.01 s
355 K
(J)
360 K
(K)
365 K
(L)
370 K
(M)
375 K
(N)
380 K
(O)
385 K
(P)
390 K
1 J K-1 g-1
Specific Heat Capacity
Temperature in K
300
350
400
450
500
550
600

110

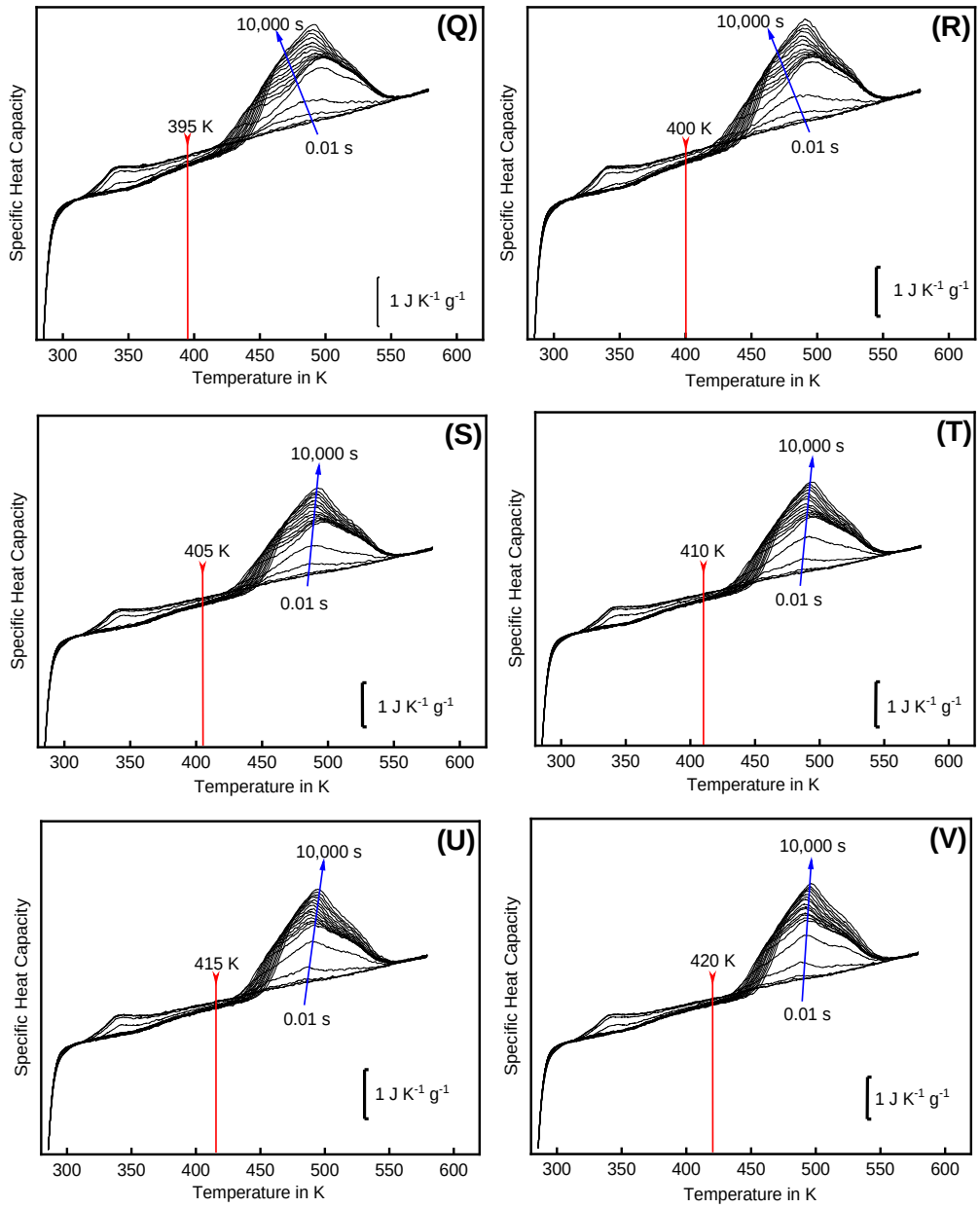

Figure S6 FSC heating scans of PA 66 after isothermal annealing at different temperatures for different times between 0.01 s and 100,000 s, as indicated in the legend. The heating rate is 10,000 K s^{-1}, and the vertical arrow indicates the temperature of prior annealing.

As illustrated in Figure S7, the nucleation kinetics can be investigated by analyzing the enthalpy change due to cold-crystallization in the heating scans of Figure S6. The dependence of the cold-crystallization enthalpy on annealing time have been fitted by a double Avrami function, as described in Eq.(1) of the main text. The half-time of nucleation, $t_{half,nucl}$, can be obtained through this double Avrami fit.

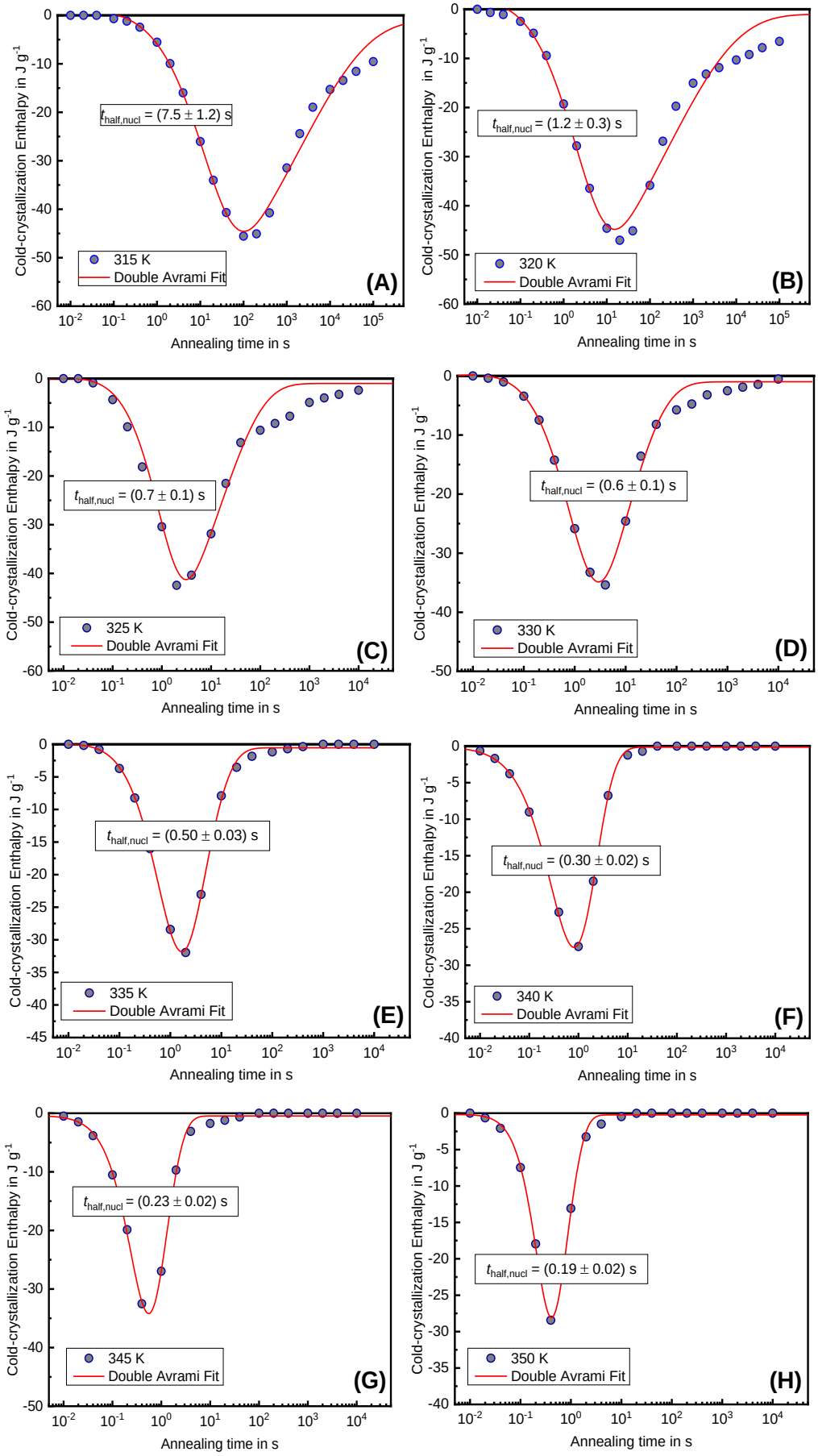
(A)
$t_{half,nucl}$ = (7.5 ± 1.2) s
315 K
Double Avrami Fit
(B)
$t_{half,nucl}$ = (1.2 ± 0.3) s
320 K
Double Avrami Fit
(C)
$t_{half,nucl}$ = (0.7 ± 0.1) s
325 K
Double Avrami Fit
(D)
$t_{half,nucl}$ = (0.6 ± 0.1) s
330 K
Double Avrami Fit
(E)
$t_{half,nucl}$ = (0.50 ± 0.03) s
335 K
Double Avrami Fit
(F)
$t_{half,nucl}$ = (0.30 ± 0.02) s
340 K
Double Avrami Fit
(G)
$t_{half,nucl}$ = (0.23 ± 0.02) s
345 K
Double Avrami Fit
(H)
$t_{half,nucl}$ = (0.19 ± 0.02) s
350 K
Double Avrami Fit
Cold-crystallization Enthalpy in J g^{-1}
Annealing time in s

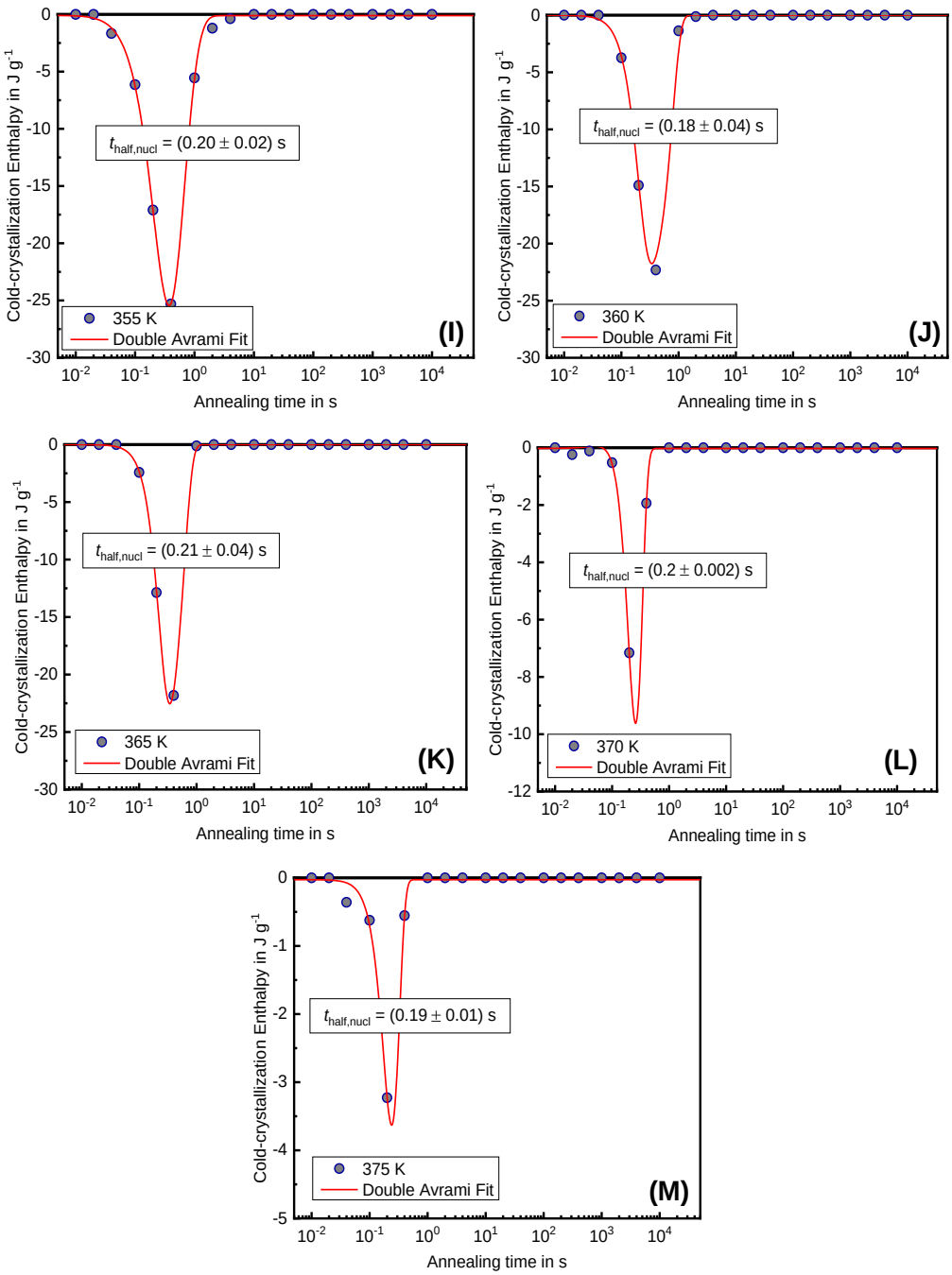

Figure S7 Cold-crystallization enthalpy at different temperatures; (A) 315 K, (B) 320 K, (C) 325 K, (D) 330 K, (E) 335 K, (F) 340 K, (G) 345 K, (H) 350 K, (I) 355 K, (J) 360 K, (K) 365 K, (L) 370 K, (M) 375 K. The data are fitted by a double Avrami equation (see Eq.1 in main text).

Figure S8 shows the total enthalpy change from the heating scans in Figure S6. The fit with the Avrami function including secondary crystallization, Eq.(2) of the main text, provides the half-time of crystallization.

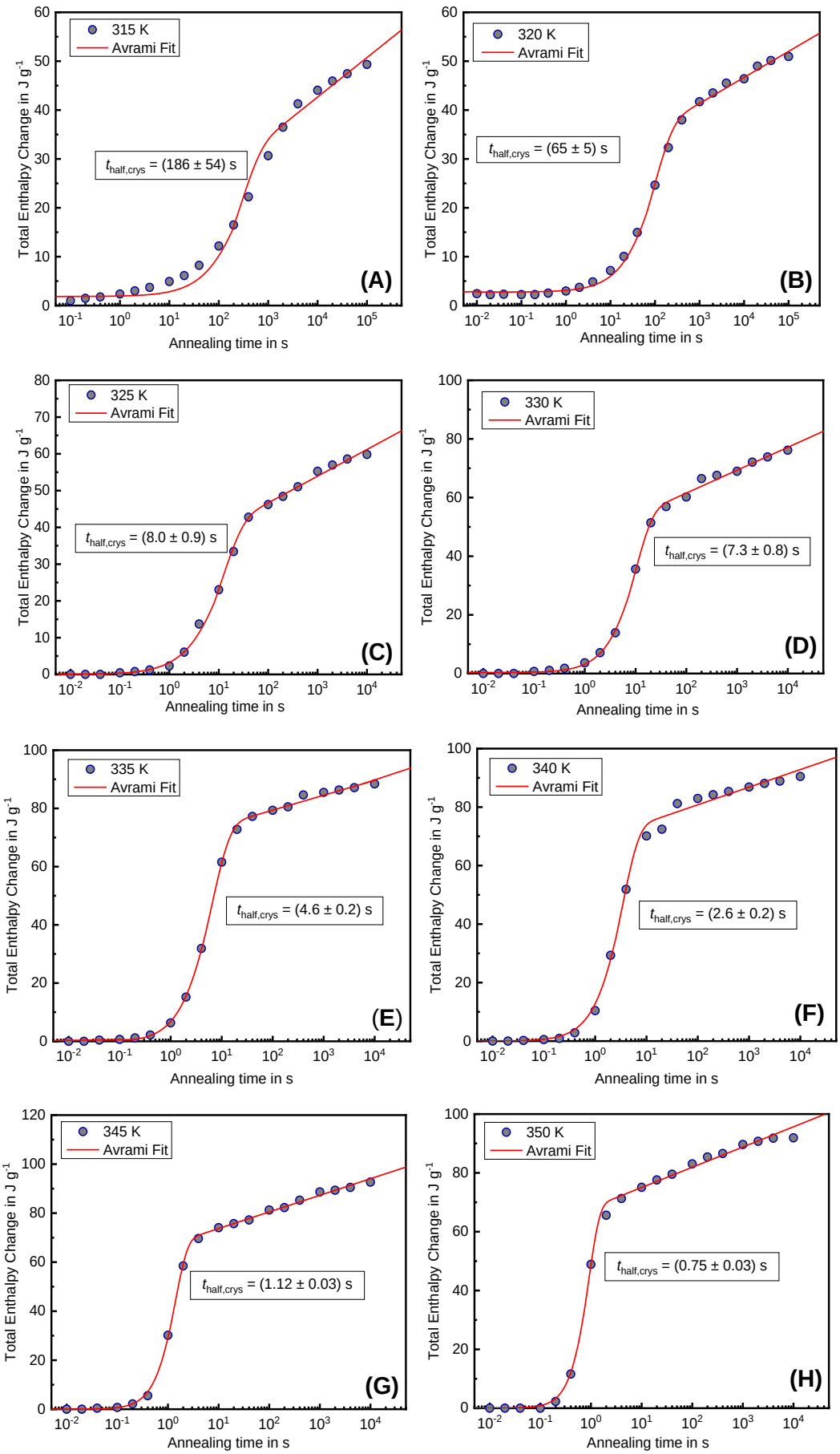
315 K
Avrami Fit
$t_{half,crys}$ = (186 ± 54) s
(A)
320 K
Avrami Fit
$t_{half,crys}$ = (65 ± 5) s
(B)
325 K
Avrami Fit
$t_{half,crys}$ = (8.0 ± 0.9) s
(C)
330 K
Avrami Fit
$t_{half,crys}$ = (7.3 ± 0.8) s
(D)
335 K
Avrami Fit
$t_{half,crys}$ = (4.6 ± 0.2) s
(E)
340 K
Avrami Fit
$t_{half,crys}$ = (2.6 ± 0.2) s
(F)
345 K
Avrami Fit
$t_{half,crys}$ = (1.12 ± 0.03) s
(G)
350 K
Avrami Fit
$t_{half,crys}$ = (0.75 ± 0.03) s
(H)
Total Enthalpy Change in J g^{-1}
Annealing time in s

140

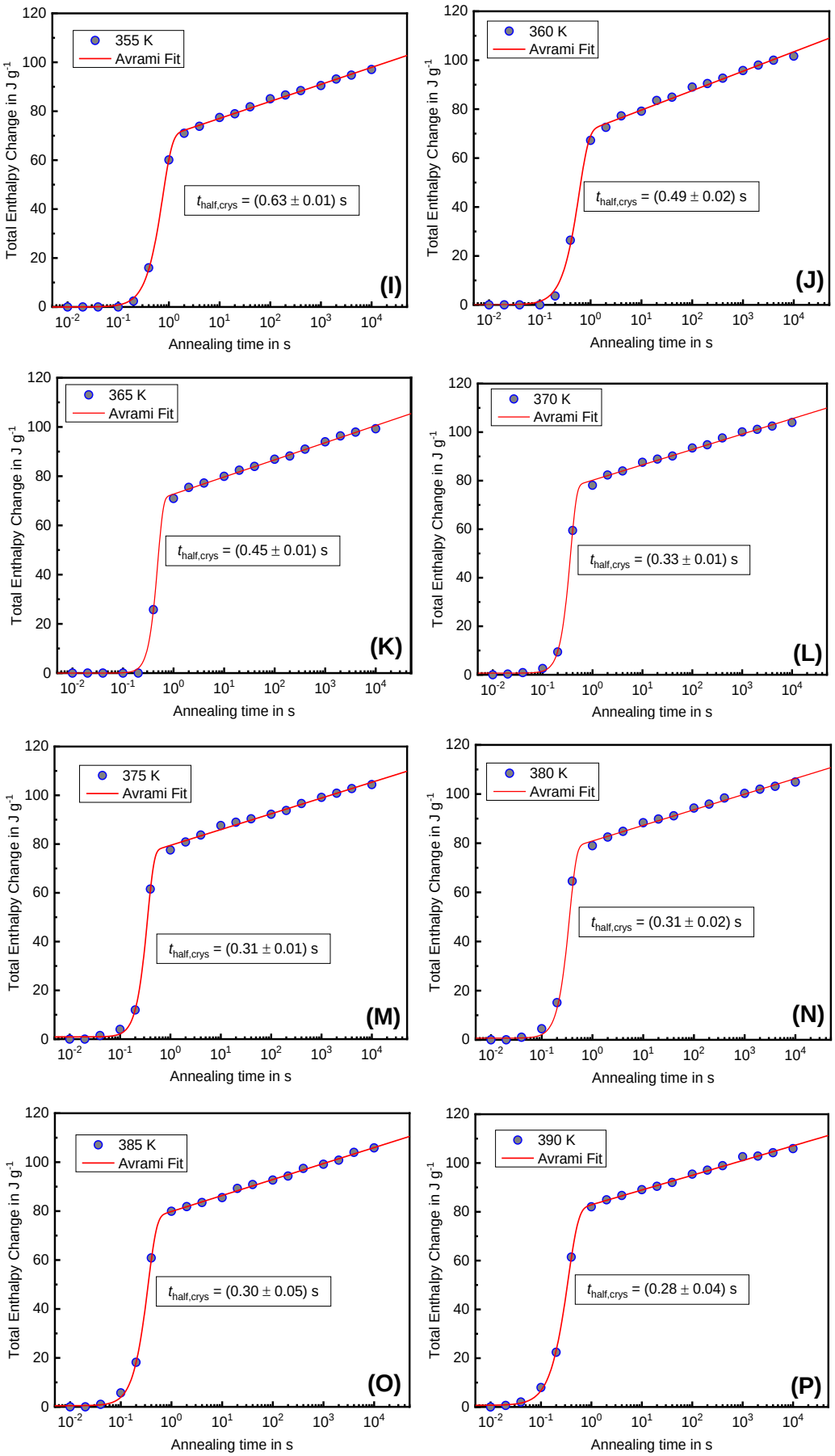
355 K
Avrami Fit
$t_{half,crys}$ = (0.63 ± 0.01) s
(I)
360 K
Avrami Fit
$t_{half,crys}$ = (0.49 ± 0.02) s
(J)
365 K
Avrami Fit
$t_{half,crys}$ = (0.45 ± 0.01) s
(K)
370 K
Avrami Fit
$t_{half,crys}$ = (0.33 ± 0.01) s
(L)
375 K
Avrami Fit
$t_{half,crys}$ = (0.31 ± 0.01) s
(M)
380 K
Avrami Fit
$t_{half,crys}$ = (0.31 ± 0.02) s
(N)
385 K
Avrami Fit
$t_{half,crys}$ = (0.30 ± 0.05) s
(O)
390 K
Avrami Fit
$t_{half,crys}$ = (0.28 ± 0.04) s
(P)
Total Enthalpy Change in J g^{-1}
Annealing time in s

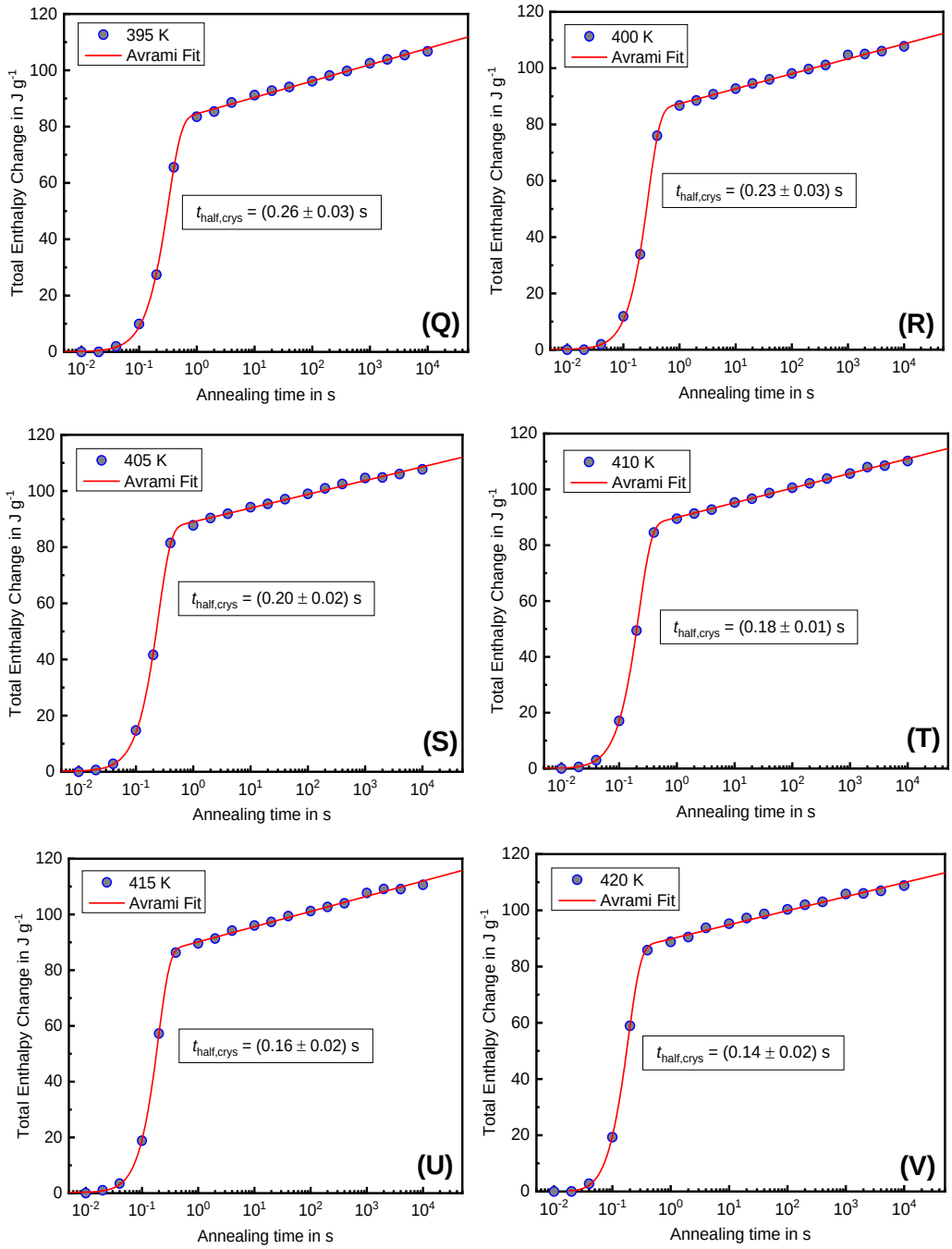

Figure S8 Total enthalpy change as function of annealing time after annealing at different temperatures as indicated in the legends. The data are fitted by the Avrami equation (Eq.(2) in the main text).

Section 5: Estimating the steady state nucleation rate, J_{st}, through isothermal FSC experiments

By using Eq.(9) of the main text, the dependence of $N_v(t)$ on annealing time can be estimated through the cold-crystallization enthalpy. Then, with a fit to Eq.(6) of the main text, the steady-state nucleation rate can be obtained from the data in Figure S9 .

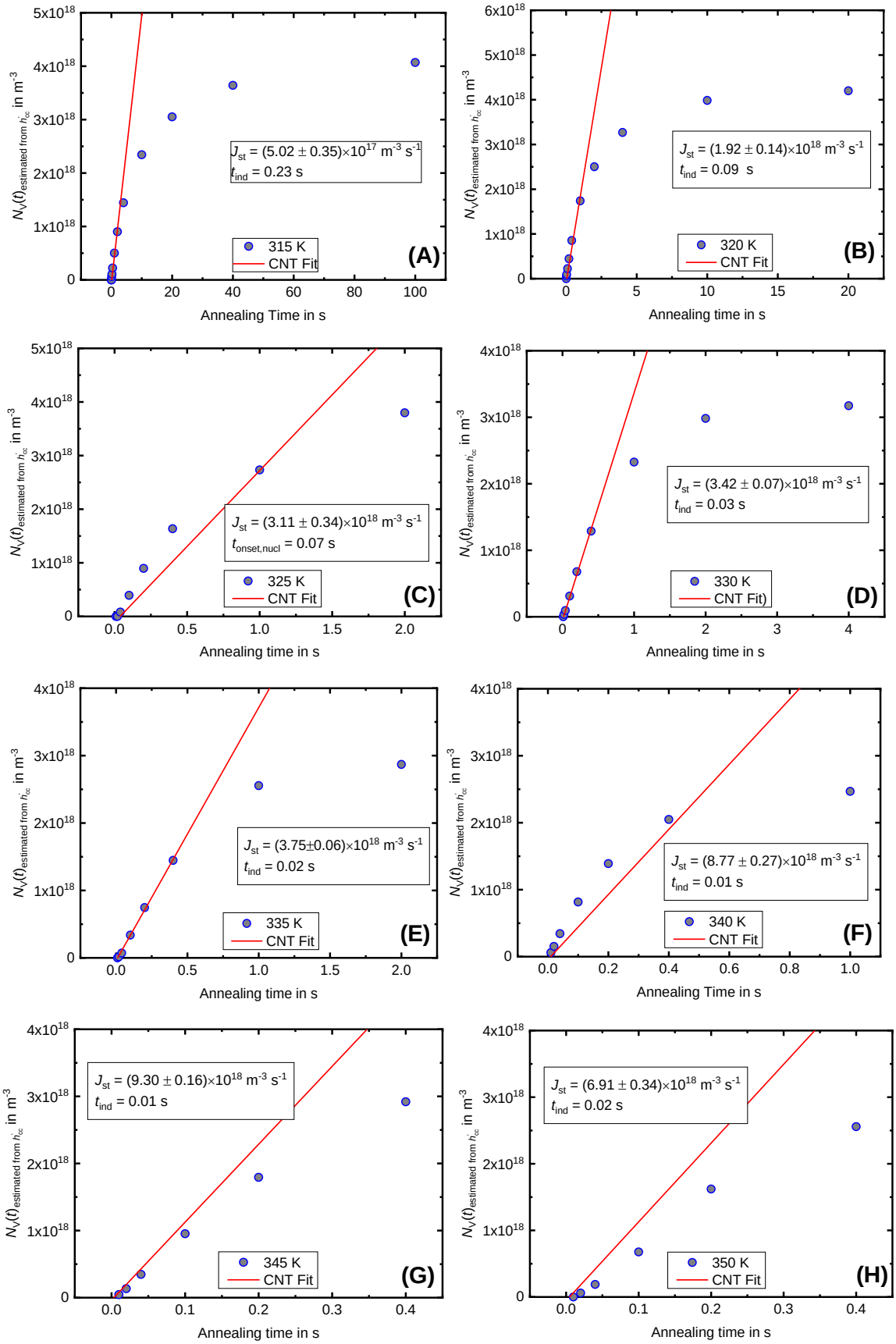
(A)
J_{st} = (5.02 ± 0.35)×10^{17} m^{-3} s^{-1}
t_{ind} = 0.23 s
315 K
CNT Fit
(B)
J_{st} = (1.92 ± 0.14)×10^{18} m^{-3} s^{-1}
t_{ind} = 0.09 s
320 K
CNT Fit
(C)
J_{st} = (3.11 ± 0.34)×10^{18} m^{-3} s^{-1}
$t_{onset,nucl}$ = 0.07 s
325 K
CNT Fit
(D)
J_{st} = (3.42 ± 0.07)×10^{18} m^{-3} s^{-1}
t_{ind} = 0.03 s
330 K
CNT Fit)
(E)
J_{st} = (3.75±0.06)×10^{18} m^{-3} s^{-1}
t_{ind} = 0.02 s
335 K
CNT Fit
(F)
J_{st} = (8.77 ± 0.27)×10^{18} m^{-3} s^{-1}
t_{ind} = 0.01 s
340 K
CNT Fit
(G)
J_{st} = (9.30 ± 0.16)×10^{18} m^{-3} s^{-1}
t_{ind} = 0.01 s
345 K
CNT Fit
(H)
J_{st} = (6.91 ± 0.34)×10^{18} m^{-3} s^{-1}
t_{ind} = 0.02 s
350 K
CNT Fit
$N_V(t)_{estimated\ from\ h'_{cc}}$ in m^{-3}
Annealing Time in s
Annealing time in s

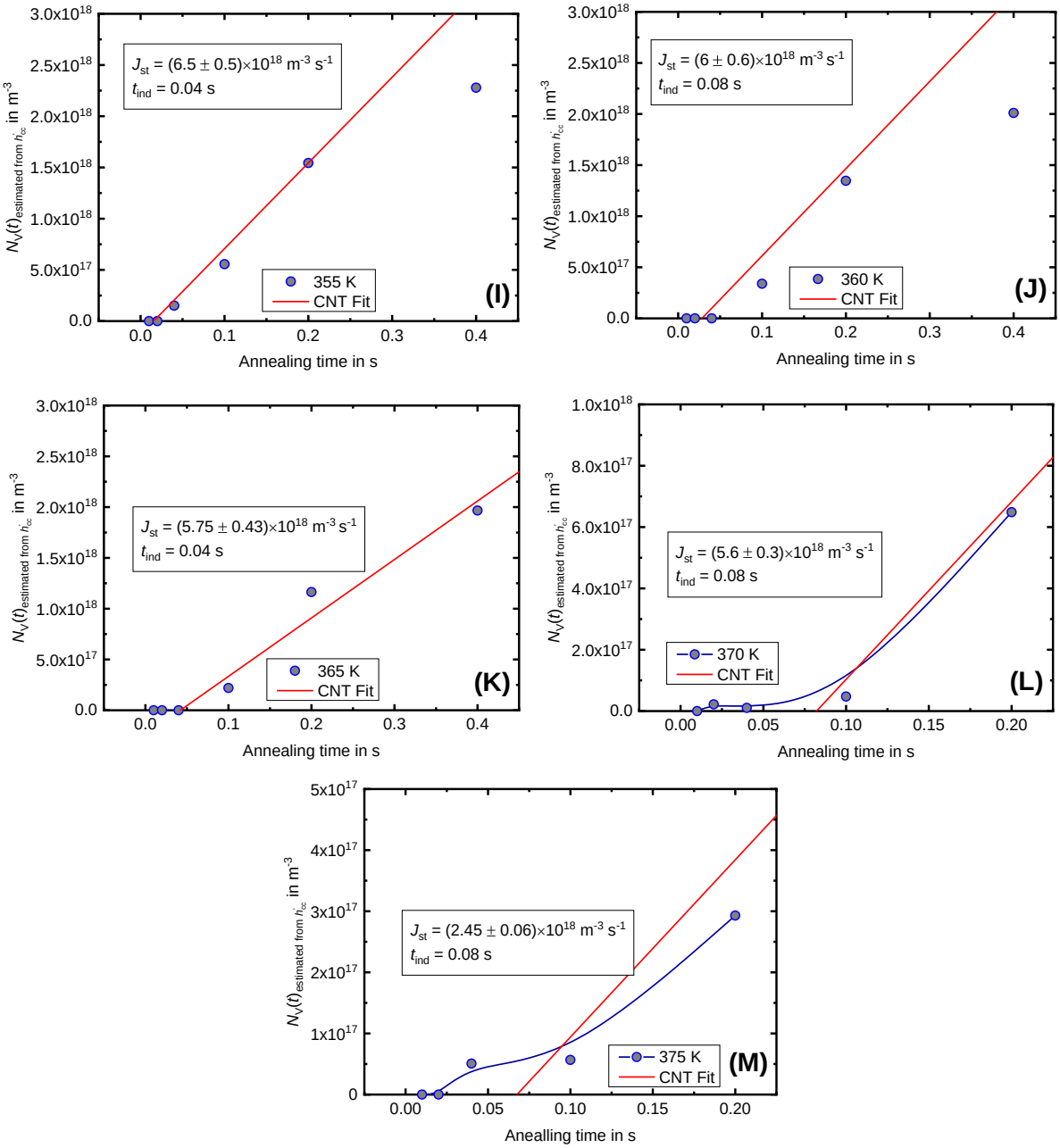

Figure S9 Estimated nuclei number $N_V(t)$ as a function of the annealing time at temperatures from 315 K to 375 K; (A) 315 K, (B) 320 K, (C) 325 K, (D) 330 K, (E) 335 K, (F) 340 K, (G) 345 K, (H) 350 K, (I) 355 K, (J) 360 K, (K) 365 K, (L) 370 K, (M) 375 K. The data are fitted by the CNT expression for the steady-state nucleation rate (Eq.(6) in the main text).

References

1. McKinney, M. L., Estimating Volumetric Fossil Abundance from Cross-Sections: A Stereological Approach. *PALAIOS* **1986,** *1* (1), 79-84.